Recent Improvements to the Keck II Laser Guide Star Facility

S. Ragland, J. Chin, P. Wizinowich, S. Cetre, S. Lilley, E. Wetherell, D. Medeiros and R. Rampy

[a]W. M. Keck Observatory, 65-1120 Mamalahoa Hwy, Kamuela, HI 96743

Email: sragland@keck.hawaii.edu

ABSTRACT

The laser guide star (LGS) adaptive optics (AO) system on the Keck II telescope has been upgraded with a Center Launch Laser System (CLS) and a next generation laser (NGL; i.e. a TOPTICA/MPBC laser) is being implemented. The purpose of the CLS upgrade is to improve the performance of the existing Keck II LGS AO system by reducing the perspective elongation of the LGS as seen by the AO wavefront sensor and hence the measurement error, one of the largest terms in the current error budget. This performance improvement is achieved by projecting the laser from behind the Keck telescope's secondary mirror instead of from the side of the Keck telescope. The purpose of the NGL upgrade is to increase the laser return and improve laser operability for science operation. The higher return from the NGL would open up new possibilities for further AO upgrades such as a laser asterism to reduce the focal anisoplanatism, and to increase the wavefront sensor (WFS) sampling rate to reduce the bandwidth error in addition to reducing the measurement error.

The CLS transitioned to science operation in June 2015. The NGL with the CLS had first light on Dec. 1, 2015 and is being optimized to support transitioning to science operations in April 2016. This paper provides an overview of the design, implementation and on-sky performance of the new launch system and laser. The results are discussed in the context of AO for extremely large telescopes.

Keywords: adaptive optics, laser guide star, center launch system, TOPTICA/MPBC laser, Strehl ratio, W. M. Keck Observatory

1. INTRODUCTION

W. M. Keck Observatory (WMKO) was the first to implement both natural guide star (NGS) and laser guide star (LGS) AO systems on a large telescope (Wizinowich et al., 2000; 2006) in order to achieve angular resolutions in the near-infrared that match the capabilities of the Hubble Space Telescope in the visible. Over 600 refereed science papers have been produced using the Keck AO systems. In addition to providing the first NGS and LGS AO facilities on a large telescope, WMKO has endeavored to continually improve the capabilities of these systems. One such improvement is the upgrade of the Keck II LGS facility.

The LGS facility upgrade has been implemented in two phases: (1) replacement of the side launch system (SLS) with a center launch system (CLS; Chin et al., 2014) and (2) replacement of the dye laser with a TOPTICA/MPBC laser (Enderlein et al., 2014) – referred to as the next generation laser (NGL) throughout this paper. A phased implementation was used to minimize the impact on day-to-day science operations and eliminate telescope downtime.

The CLS system was commissioned and handed over to science operation in mid-June 2015 for about 3.5 months of science operation until the Keck II LGS system was shut down for the integration of the NGL in early October 2015. The dye laser was replaced with the NGL and achieved its first light on Dec. 1, 2015 delivering a factor of ~ 19 higher laser returns than that of the center launched dye laser. The CLS provides more compact and symmetric laser guide star compared to the SLS.

This paper aims to give a broad view of the progress achieved in implementing the CLS and the NGL capabilities. The outline of the paper is as follows: The system overview is briefly described in Section 2, on-sky performance in Section 3, and a brief summary and future plans are provided in Section 4.

2. SYSTEM OVERVIEW

The major subsystems of the CLS are (1) a launch telescope (LT) that goes behind the secondary module, (2) a beam transport optics bench (BTOB) to condition and steer the beam that is mounted to the LT, (3) a beam transportation system (BT) to relay the laser from the laser table (located on the elevation ring) to the BTOB, and (4) associated control and operational software. The BTOB and BT include various sensor and actuators to allow remote positioning of the beam. A Safety System monitors the entire LGS facility and will take corrective action in event of a problem. A schematic diagram of the CLS and the NGL is shown in Figure 1. The CLS subsystems are presented in subsections 2.1 through 2.4 and the NGL is presented in subsection 2.5.

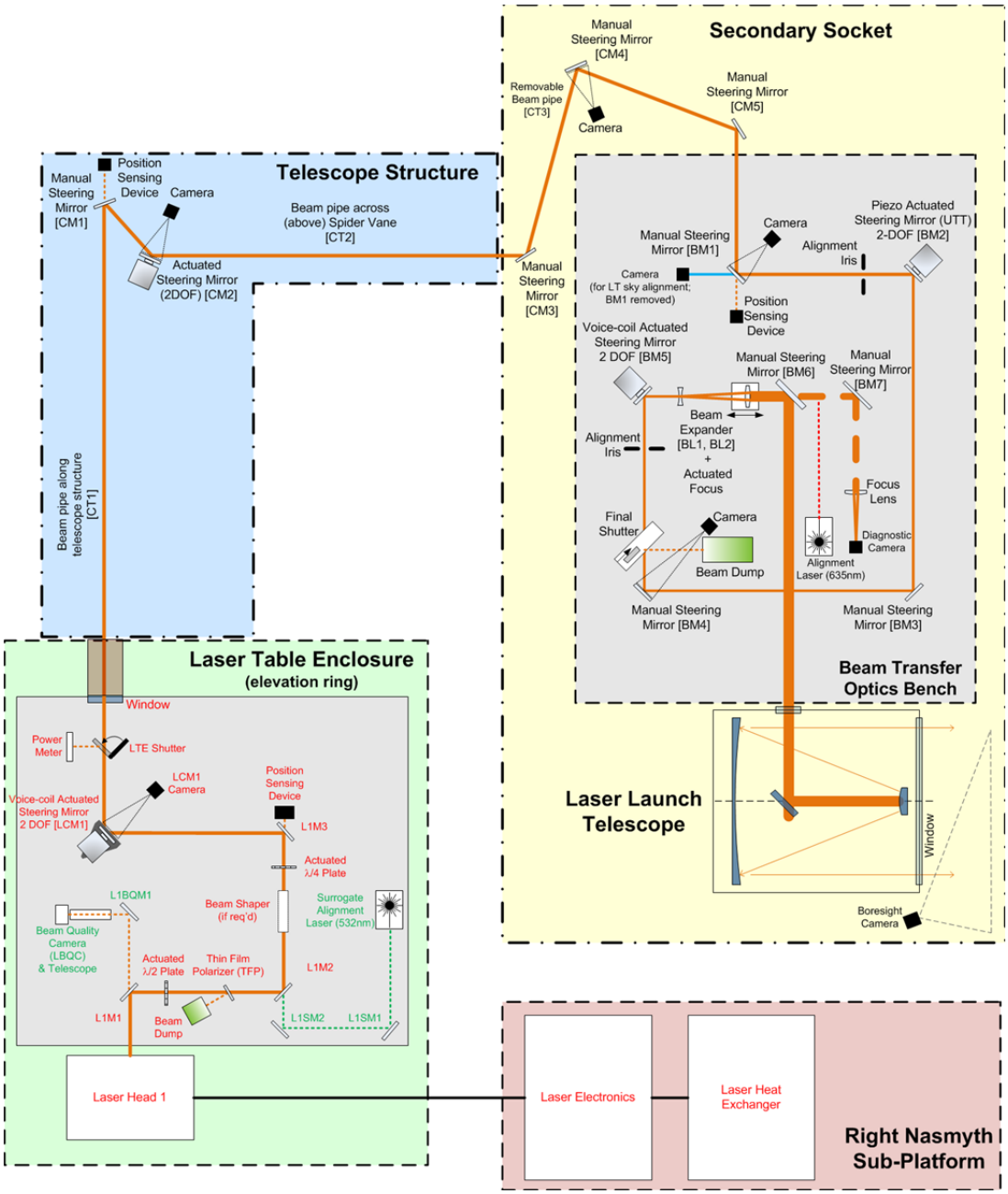

Figure 1: Schematic diagram of the K2 center launch system and the new laser

2.1 Launch Telescope (LT)

The LT provides a 12.5x beam magnification for the laser beam. The expected output Gaussian intensity profile with $1/e^2$ diameter is ~ 360 mm. A drawing of the LT is shown in Figure 2 (left) and a photograph of the launch telescope installed on to the secondary module is shown in Figure 2 (right).

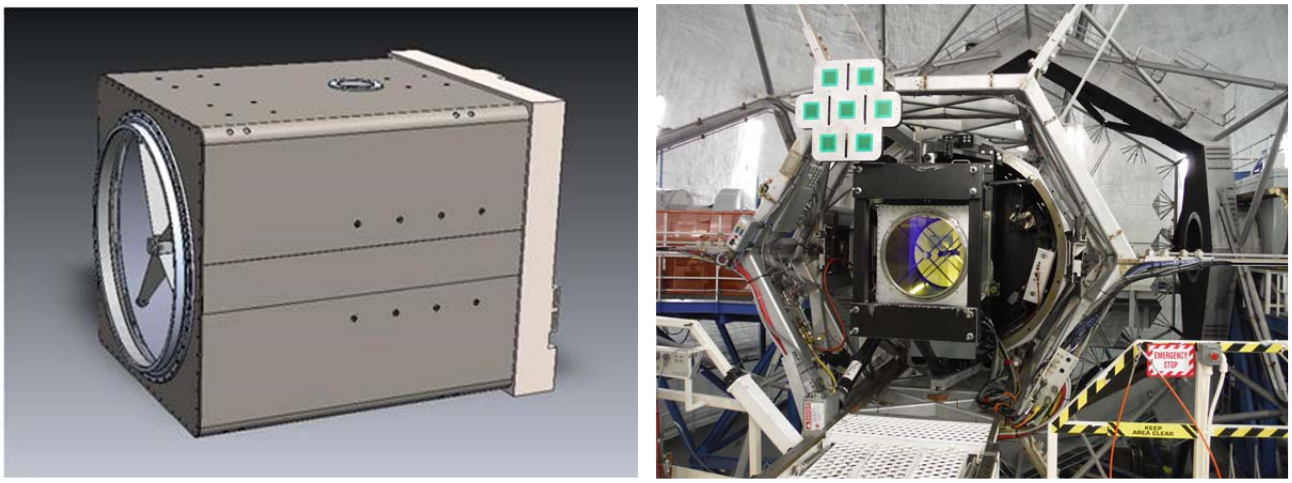

Figure 2: Left: CAD model of the launch telescope. The entrance window of the LT is seen at the top of the LT and the exit window at left. Right: The launch telescope mounted behind the telescope secondary mirror in the top end module. Note that a transponder-based aircraft detector (TBAD) is seen in the top-left (green squares).

2.2 Beam Transport Optics Bench (BTOB)

The BTOB (Figure 3) is mounted to the LT via three kinematic defining points as shown in the left figure; the output beam to the LT exits through the bottom of the plate in Figure 3 (left) and through the LT entrance window shown in Figure 2 (left). The BTOB provides 4.5x beam expansion and enables laser steering and flexure compensation using two fold mirrors BM2 & BM5. BM2 also acts as the fast up-link tip tilt mirror (UTT). The two stages work together to provide the needed travel. The UTT has a ±1.5 mrad range and BM5 has a ±13 mrad range. The laser steering range is limited by the field of view of the LT to about ± 90" on the sky but the laser steering range is limited by other factors. BL2 stage is actuated enabling focus optimization at the sodium height.

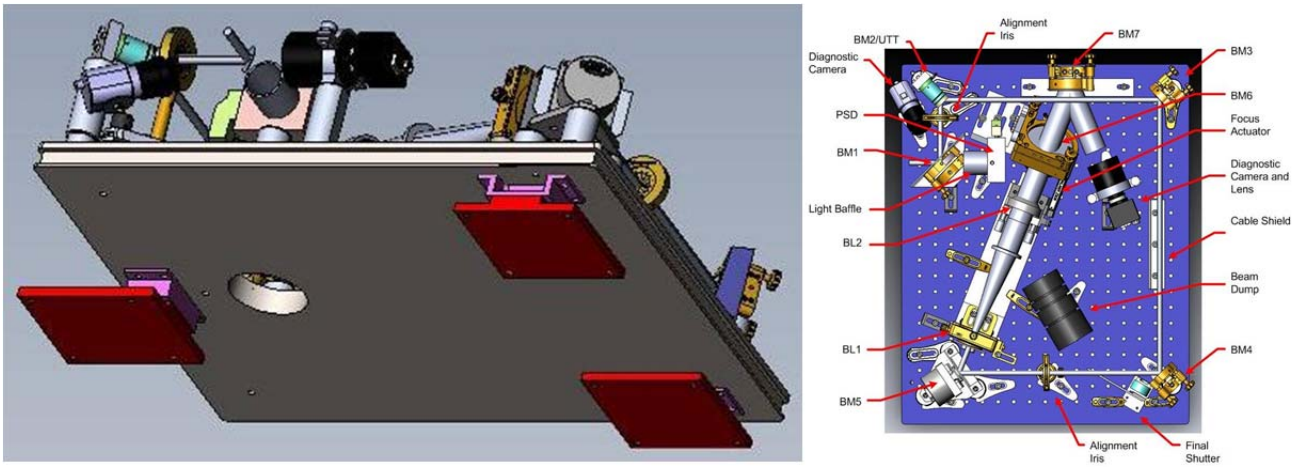

Figure 3: Left: The bottom view of the BTOB. The beam exits through the hole seen at the bottom-left to the LT tertiary mirror. Right: Optical layout of the BTOB. The beam enters from the left to BM1 and is folded to the LT tertiary by BM6.

2.3 Beam Transport System (BT)

The beam transportation system (BT) relays the laser from the laser table, located on the elevation ring, to the BTOB, located in the secondary socket. Figure 4 (left) shows the beam-train from the laser enclosure at the bottom-left (multi-colored rectangles) to the BTOB in the secondary module at the top middle. Enclosed beam tubes (CT1 through CT5) are used to transport the beam to minimize stray light entering the telescope/instrument. The enclosures also protect the optics from dust deposition. There are five fold mirrors along the beam-train (CM1 through CM5). Some of them are remotely steerable. The steering mirrors, along with position sensitive devices (PSD), and cameras are used to keep the beam centered on the entrance of the BTOB and along the beam tubes to prevent vignetting as the telescope moves in elevation. One such steering station is shown in Figure 4 (right).

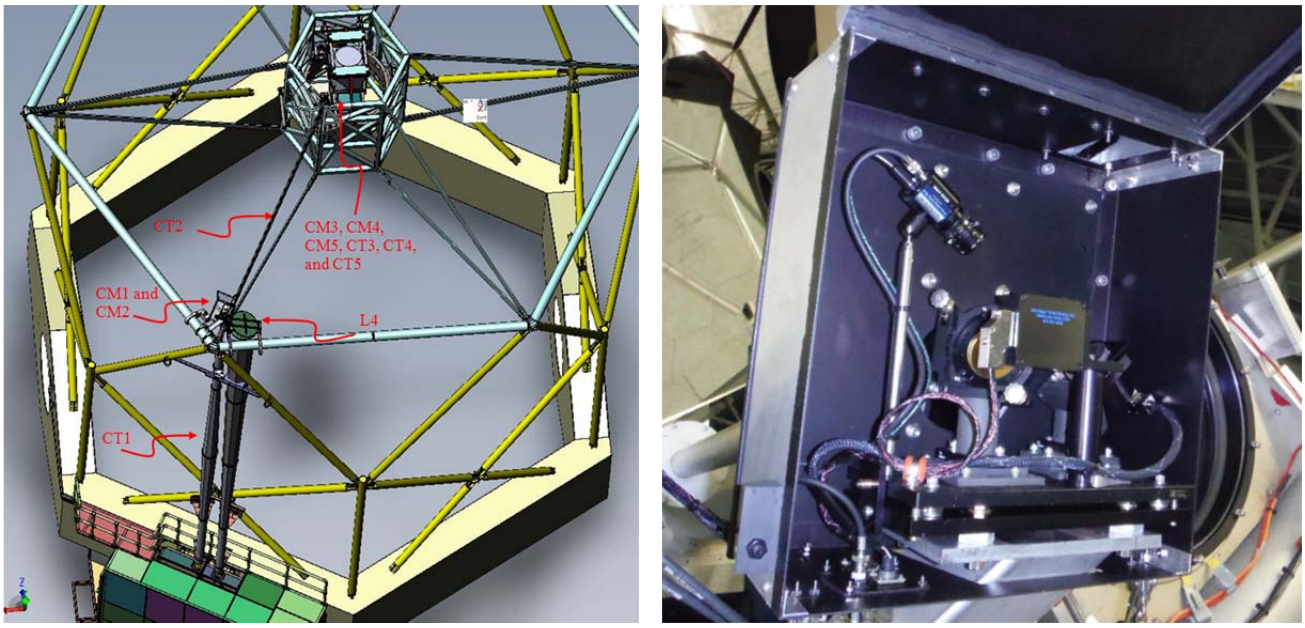

Figure 4: Left: The telescope structure showing the laser enclosure on the elevation ring (at the bottom-left) and the LT in the secondary socket (top-middle). The beam tubes are marked as CT1 through CT5. Also shown in this picture is the side-launch system (SLS); the exit lens is marked as L4. Right: The junction box that fold the beam from the laser table to the secondary module behind the shadow of one of the spiders. It houses the fold mirrors CM1 and CM2, an alignment camera, and a PSD.

2.4 Software

The software includes control software to align/steer the laser, propagate the laser, interface software to the laser safety system and the telescope and AO system, and higher level software tools primarily written in IDL.. There are five major control loops in the system, namely, (1) telescope flexure correction performed by TM2 (laser enclosure to the top end of the telescope), (2) secondary flexure correction performed by CM2 (across the primary mirror behind one of the spiders), (3) up-link tip-tilt correction performed by the UTT (to apply TT correction for the laser), (4) laser pointing and CLS flexure compensation performed by coordinated moves of the BM2 and BM5 mirrors (to steer the beam in the science field with respect the Keck telescope pointing), and (5) focus control of the output beam performed by the beam expander stage. A schematic diagram of the control software is shown in Figure 5 where the control loops are numbered in black.

The high level software includes a sequencer written in Python to align/propagate the laser in conjunction with safety system software, and IDL tools to calculate the sodium height and thickness in order to update the WFS focus model, determine LT pointing offset at the zenith to update laser pointing model, search the field to acquire the laser on the wavefront sensor, measure laser spot characteristics and LGS AO performance in terms of image quality for science, update WFS centroid offsets based on input from the low bandwidth truth wavefront sensor, and update variable centroid gain for the sub-apertures based on the laser spot characteristics.

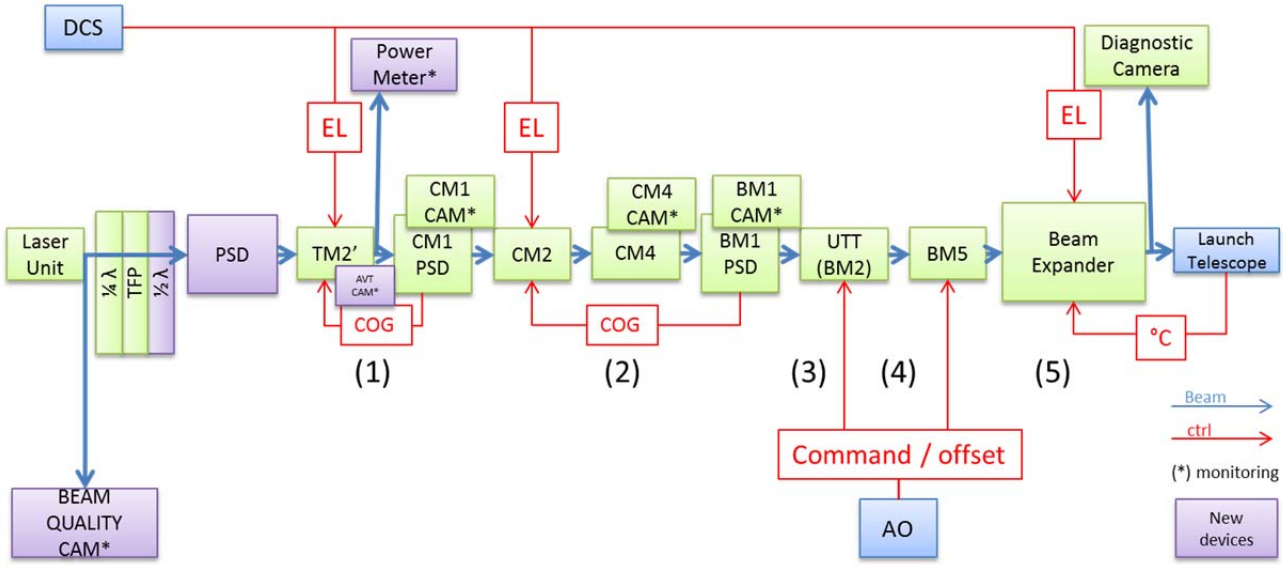

Figure 5: A schematic diagram of the control software showing different control loops (labeled in black) and associated devices.

2.5 Next Generation Laser (NGL)

The dye laser has been replaced with a Raman-fiber amplifier (RFA) laser provided by a consortium of TOPTICA and MPBC (Figure 6). The new laser is a continuous wave Raman fiber amplifier with diode pumping and second harmonic generation of the sodium wavelength. It has the capability for optical repumping of the D2b line and detuning of the central wavelength for Rayleigh background subtraction. The laser head, on the elevation ring with a changing gravity vector, produces ~22W.

The startup time of the laser depends on the temperature of the system. Due to the cold dome environment (-2°C to 2°C) a cold startup requires 4 to 5 hours in order for internal components to stabilize. Once the system is warm (15°C), the laser can be started in 5 minutes, making it ideal for time domain astronomy. The laser system temperature is maintained by a coolant heat exchanger and heaters in the system once the temperature is stable. Heat from the laser is removed from the telescope via the observatory's glycol coolant system. Additional calibrations such as wavelength and health checks do increase the startup time. These calibrations are daytime maintenance activities, not performed during normal nighttime operations.

TOPTICA/MPBC provides two configurations of RFA pumping, local and remote. WMKO uses the remote pumping which allows the laser head/RFA to be tens of meters away from the pump diodes via long fibers. ESO, who also has TOPTICA/MPBC lasers, uses the local pumping configuration where the laser head and RFA are only a few meters apart. The remote pumping requires ~ 8% more pump diode power to overcome the fiber losses; thus reducing the diode lifetime slightly. The software for the laser enables easy monitoring of the health and diagnostics of subsystems within the laser. The TOPTICA/MPBC laser is a highly efficient laser system taking relatively low power (~ 1200 W compared to ~ 80 kW for the dye laser system including cooling) while the output power is higher for the new laser (~22 W against 14 W for the dye laser).

Figure 6: Left: The old dye laser amplifier table enclosure (the large rectangular unit in black). Middle: The new TOPTICA/MPBC laser (the white unit in the middle) and new laser table (black unit above the laser). The fiber splice boxes can be seen on the mid-left. The design of the laser head and new laser table allows the addition of two more lasers to support future AO upgrades. Right: The new laser table with fore-optics relaying the laser beam to the CLS.

To support the new laser electronics and the heat exchanger, a new sub-platform was installed under the right Nasmyth platform (Figure 7). The sub-platform can support up to three TOPTICA/MPBC lasers for potential future expansion of the Keck II LGS facility.

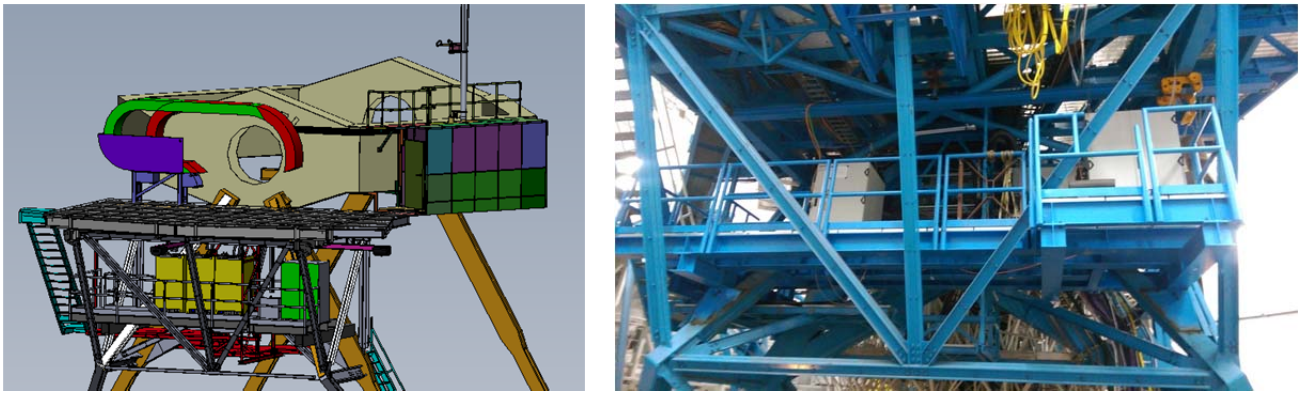

Figure 7: A new sub-platform to support the new laser electronics and the heat exchanger. Left: A drawing of the sub-platform showing three laser electronics racks (yellow units) and the heat exchanger (green unit). Right: A photograph of the sub-platform after the installation of the first laser electronics rack and the heat exchanger.

3. ON-SKY PERFORMANCE

The on-sky performance of the laser system could be classified into two parts: (1) performance of the laser in section 3.1, and (2) performance of the LGS AO system in section 3.2.

3.1 Laser performance

The performance of the dye laser system for the two launch configurations (SLS & CLS) are compared using long term measurements taken during AO checkout (~ 5 years for the SLS and ~ 6 months for the CLS). Also included in the study is more recent NGL data taken during the initial commissioning runs over a period of about a month.

3.1.1 Laser spot size

The measured LGS spot size for the two launch configurations and the two lasers are shown in Figure 8 (left) against relative seeing. The seeing measurements were taken with the AO acquisition camera (ACAM) which has a plate scale of 0.134"/pixel); the exposure times were often short and hence the term “relative” seeing is used. The measurements correlate well with full width at half maxim (FWHM) of the open loop NIRC2 science camera exposures (when available) and hence are a good relative measure of the seeing. For comparison, the spot size measurements of the Keck I CLS and solid state laser are shown in Figure 8 (right). The CLS on both telescopes achieves < 1.5” spot size under excellent seeing conditions. Overall, the CLS spot size is ~ 24% smaller than that of the Keck II SLS.

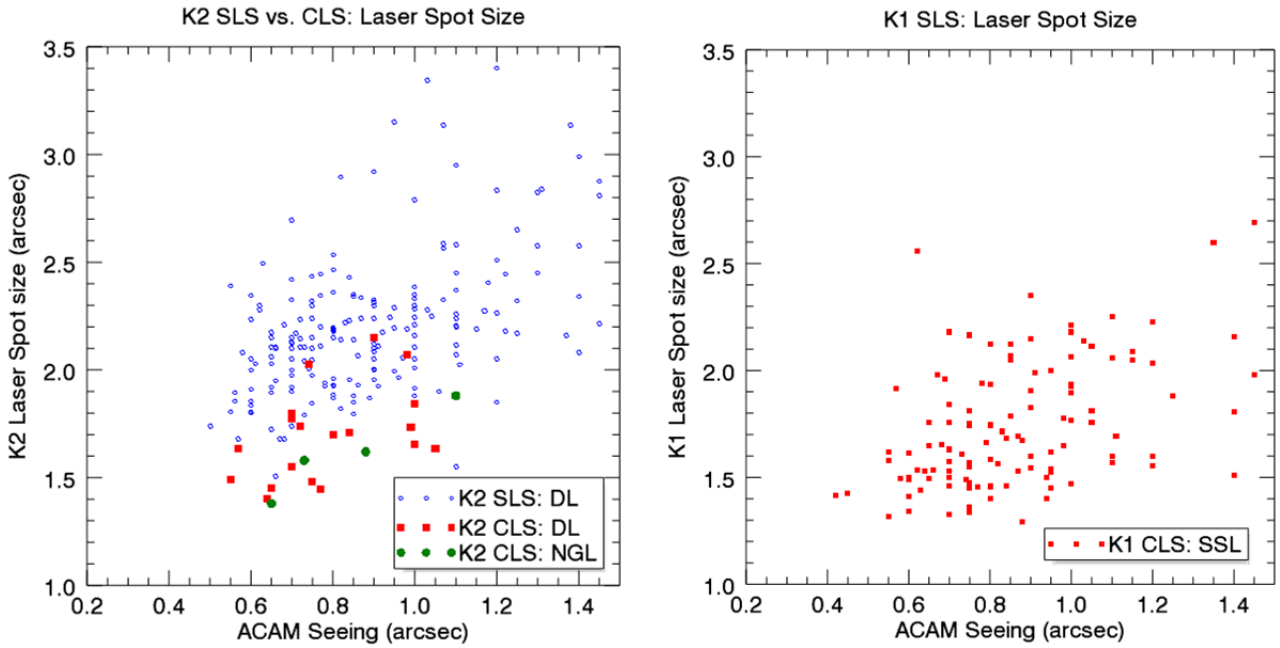

Figure 8: Laser spot size against ACAM FWHM. Left: Keck II SLS and CLS with the dye laser (DL) and CLS with the NGL. Right: K1 CLS with the solid state laser.

3.1.2 Laser spot elongation

The primary reason for switching from the SLS to the CLS is to benefit from more compact and symmetric laser spot due to reduced perspective elongation and the circular symmetry of LGS elongation on the WFS. The measured spot elongation is shown in Figure 9. The mean spot elongation of the Keck II CLS is 12% versus ~40% for the SLS.

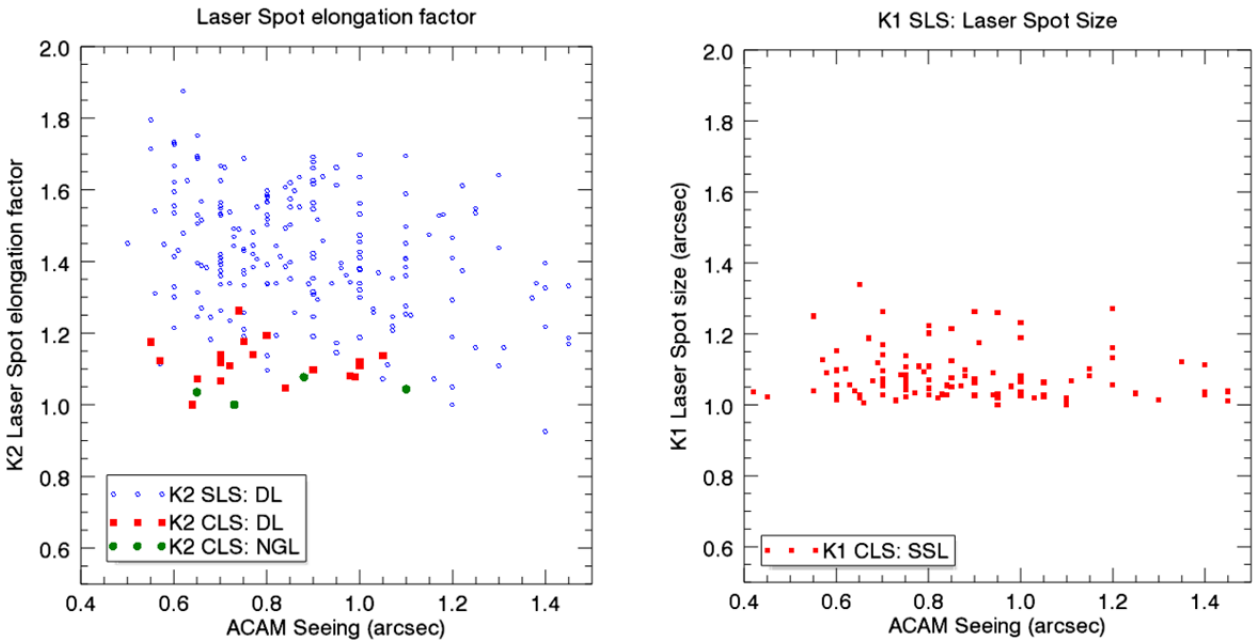

Figure 9: Laser spot elongation versus relative seeing. Left: Keck II SLS and CLS with the dye laser (DL) and CLS with the NGL. Right: Keck I CLS with the solid state laser.

In order to understand the performance of the laser in terms of spot characteristics and look for ways to improve this further if necessary, the error budget of this parameter is looked into in some detail. For this purpose, unstacked images (separate images for each telescope segment), in addition to stacked images, were taken with the acquisition camera under similar seeing condition. Figure 10 shows unstacked images of the SLS: dye laser (left) and the CLS/NGL (right). The figure clearly shows reduction in the perspective elongation with radial distance from the launch telescope.

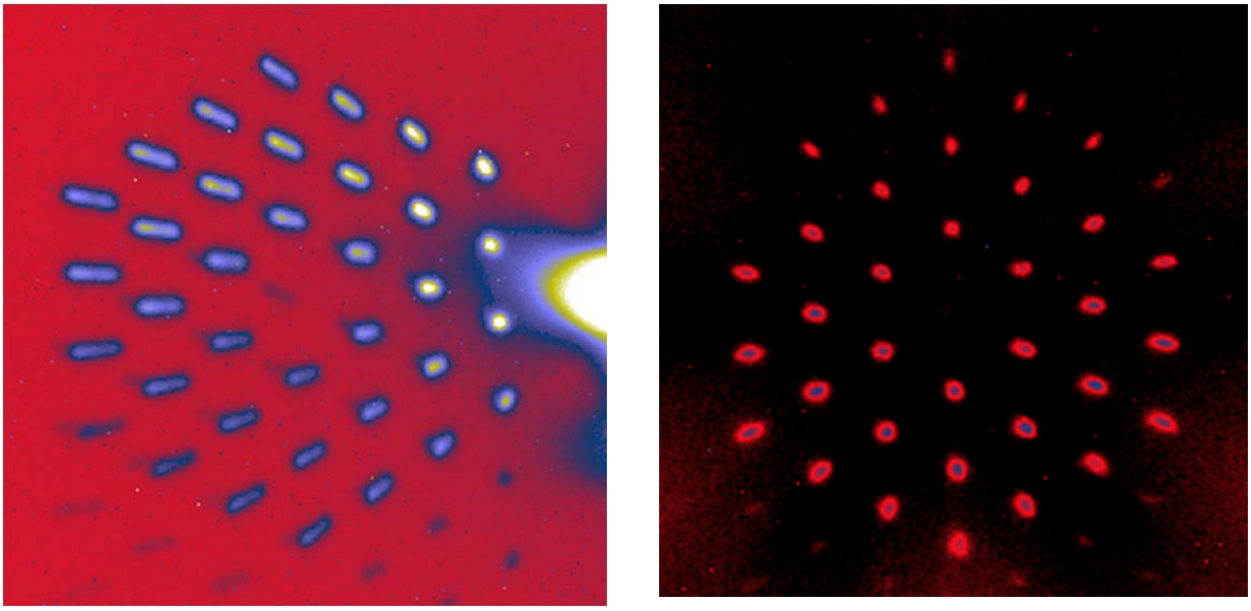

Figure 10: LGS images corresponding to the 36 unstacked primary mirror segments of the Keck telescope. The ghost images seen below are caused by a dichroic beam-splitter in the optical system. Left: SLS with the dye laser; the bright spot at the mid-right is due to Rayleigh scattering. Right: CLS with the NGL.

The laser spot size depends on factors such as sodium thickness, sodium height, atmospheric seeing, and optical effects such as diffraction from the launch telescope, laser beam quality and optical aberrations in the system. The contributions

from different terms are estimated from LGS spot size measurements (both stacked and unstacked) taken with the CLS/NGL under excellent sky condition (seeing ~ 0.5").

The sodium-thickness-free spot size is estimated from the FWHM of the unstacked images in the azimuthal direction and the value is 1.06". Now the broadening due to finite sodium thickness is computing from the sodium-thickness-free spot size and the stacked images; the value is $\sqrt{1.38^2 - 1.06^2}$ = 0.88". The broadening due to atmospheric seeing in double pass and finite beam size (Gaussian waist diameter of 0.36 m) is 0.71" and 0.34" respectively. The combination of the above three effects estimates the laser spot size, imaged with the full Keck aperture, as 1.2 ± 0.1" and the measured value under similar seeing condition is 1.38". We attribute the difference between the model and the observed spot size ($\sqrt{1.38^2 - 1.2^2}$ = 0.68") to the launch optics aberrations although contributions from other optical effects such as imperfect acquisition camera focus, imperfect laser collimation, and laser beam divergence cannot be ruled out.

The measured RMS wavefront error of the LT is 35nm and the wavefront error of the whole launch optics is estimated to be ~ 110 nm. It is difficult to estimate spot broadening from these values alone not knowing the special frequency of the wavefront aberrations. For all practical purposes we conclude that the measured spot size of ~ 1.4" under excellent seeing condition is understood.

A spot broadening model with radial distance from laser projection in the telescope primary space has been constructed to estimate sodium thickness and sodium-thickness-free spot size. Assuming the sodium height as 86.3 km, the best-fit model to the unstacked images estimates the sodium-thickness-free spot size and the sodium thickness to be 1.1 ± 0.1" and 11.4 ± 1.8 km, respectively. The sodium-thickness-free spot size estimated through the modeling is consistent with the estimated from FWHM of the unstacked images in the azimuthal direction (1.06").

The best-fit spot broadening model predicts the spot elongation for the outer sub-apertures of the Keck wavefront sensor as 1.86” and the corresponding value for the TMT would be ~3.6” (a portion of the unstacked images on one side of the TMT primary in CLS configuration would look somewhat similar to the unstacked Keck SLS images (Figure 10 left) although the number density of the segments are very different). By stacking the best-fit model images, the model full-aperture spot size for the Keck telescope is estimated to be 1.34" which is consistent with the measured value of 1.38". The corresponding value for TMT would be ~1.7". The relatively large laser spot size could potentially limit the sensitivity of the WFS for LGS (in comparison to the NGS of similar brightness) for the next generation telescopes such as TMT and GMT. Moreover, the relatively large field stop required for the elongated outer sub-apertures of the WFS could result in increased Rayleigh background.

3.1.3 Laser brightness

The brightness of the dye laser in the SLS and CLS configurations at higher elevations is compared with the NGL brightness. Figure 11 (left) is a plot of normalized frequency versus equivalent R magnitude of the LGS. The median brightness of the dye laser in SLS configuration for high elevation targets (Elevation: 70-87°), based on 2728 measurements taken during Apr. 2013 through Jun. 2015, is R = 10.2 $\pm$ 0.4. The median brightness of the dye laser in CLS configuration for high elevation targets (Elevation: 70-87°), based on 750 measurements taken during Apr. 2014 through Oct. 2015, is R = 10.7 ± 0.4. The extra fold mirrors (19 of them) along the CLS beam-train are partially responsible for the observed throughput loss of ~ 0.5 magnitudes with the CLS in comparison to the SLS; beam clipping in the BTOB and the LT is also expected to contribute to the throughput loss. Also shown in the figure is the brightness of the NGL in CLS configuration for a narrower elevation range (Elevation: 75–87° since the return of the NGL depends heavily on pointing orientation on the sky) taken on Jan. 5, 2016 UT after optimizing the launch optics alignment and focus, and the laser wavelength and polarization. The median value from these measurements (1630 data points) is R = 7.5 $\pm$ 0.2.

The NGL brightness measurements taken at all elevations are plotted against zenith distance for different azimuth range in Figure 11(right). The elevation and azimuth dependent laser return is apparent from this figure. A 3D plot of the laser return in polar coordinates could be constructed and compared to the model estimations when more measurements covering the entire elevation and azimuth range become available.

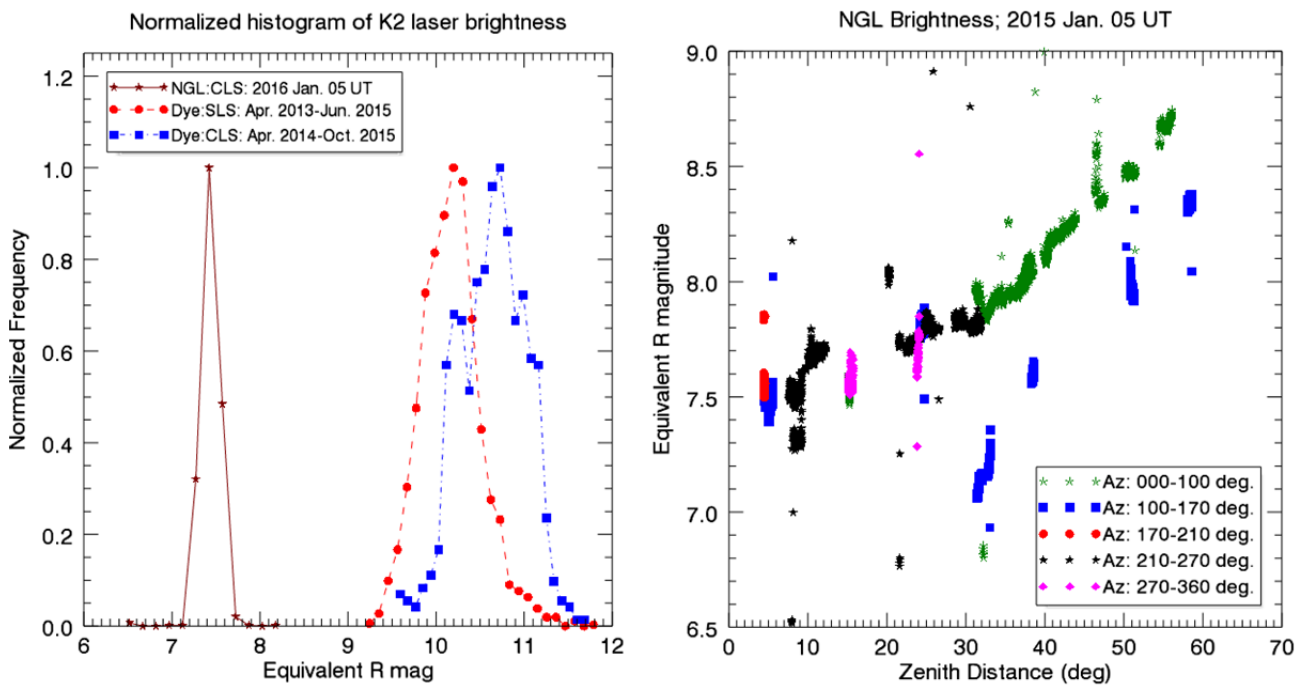

Figure 11: Left: Relative histogram of laser brightness against equivalent R magnitude for high elevation target (see the text for details.) Right: Equivalent R magnitude of the NGL with zenith distance for different azimuthal ranges for all elevations.

3.1.4 CLS Pointing

The steering of the laser on the sky is done through coordinated moves of the BM2 and the BM5 mirrors in the BTOB. The laser pointing system suffers significant flexure (~ 28" from the zenith down to ~63° zenith angle) with relatively large hysteresis - as much as ~5" (Figure 12). A finite element analysis of the LT shows 2.95" deviation over this zenith angle suggesting that the observed flexure and hysteresis probably come from the beam-train or telescope flexure.

A model is introduced to compensate for the flexure and a raster search tool is implemented to address the hysteresis. The raster tool uses the WFS counts to detect the laser spot and stop the search. There are plans to improve this tool by making use of the Rayleigh scatter on the WFS, when available, to quickly acquire the laser through a radial search instead of a systematic raster scan of the field.

While the search tool is one strategy, a better understanding of the root causes would be beneficial to the observatory. Some very recent work has discovered unexpected tilt motion of the Keck Secondary. This error couples directly to the pointing of the LT. Work to correct this problem has reduced laser pointing errors in the azimuthal axis by at least a factor of two, but did not improve the other axis (prior to this work, the hysteresis used to be ~11” in this axis.) In addition to continued investigation of the secondary mounting, work on the approach to flexure compensation is being reviewed. Currently the compensation assumes that flexure generated errors are pure angle, when in reality there may be a significant shear component to the error. If this proves true, it may be possible to implement a coordinated-variable centroid offset for the PSDs that provide beam-train position feedback, in addition to the BM5-BM2 coordinated moves, to improve laser pointing.

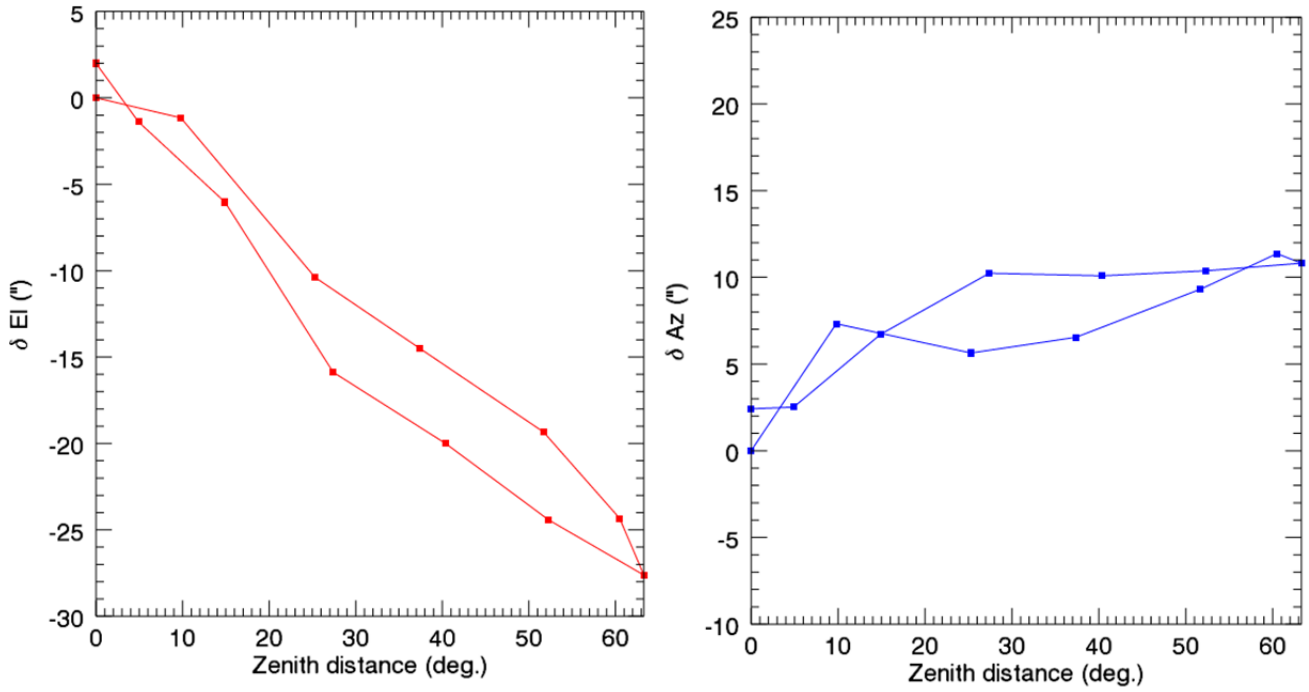

Figure 12: Laser pointing showing significant flexure and hysteresis in the system. The pointing of the telescope is systematically varied from the zenith to ~ 27° elevation and then back to the zenith to measure the flexure and hysteresis in the system.

3.1.5 Uplink tip-tilt (UTT) performance

The UTT stage limits the range of laser pointing, through coordinated moves with BM5, to ~80" which is little less than that of the launch telescope's field of view of ~90". As the flexure takes about ~30" of the range along the elevation axis and the LT pointing offset with respect to the Keck telescope at zenith takes another ~10" of the range, the available laser steering range for off-axis pointing is restricted along the elevation axis.

The UTT offloading keeps the tip/tilt mirror well within its range and the UTT residue is about 0.16".

3.2 NIRC2 LGS AO performance

The performance of the dye laser system in side launch and center launch configurations in terms of Strehl ratio and FWHM are compared using long term measurements. Also included in this section are more recent measurements taken with the NGL during one of the commissioning runs after optimizing the laser.

Figure 13 compares the performance of the CLS with that of the SLS taken during nightly AO checkouts since Aug. 2010. Overall, the Strehl and FWHM of the CLS are comparable to that of the SLS (i.e. there is no noticeable performance improvement with the CLS for standard LGS operation with the dye laser). There are not enough AO checkout data with the NGL yet.

The reduced CLS spot size (by a factor of 1.32 with respect to the SLS) would reduce the DM measurement error by the same factor since the measurement error goes linearly with the spot size. On the other hand, the reduced CLS throughput (by a factor of 1.58 with respect to the SLS) would increase the measurement error by the square-root of this factor for the photon-limited case (i.e. by a factor of 1.26). The resultant change in the measurement error of the CLS with respect to the SLS is only about 5% decrease in measurement error. Assuming that the measurement error and the total wavefront error are 150 nm and 370 nm respectively, a 5% decrease in measurement error would decrease the total wavefront error to 367 nm. The resultant K-band Strehl change would be negligible (i.e. increased from ~ 0.327 to ~0.333). This explains why we were not seeing an improvement in LGS performance with the dye laser in CLS configuration. The higher sodium return of the NGL overcomes this limitation.

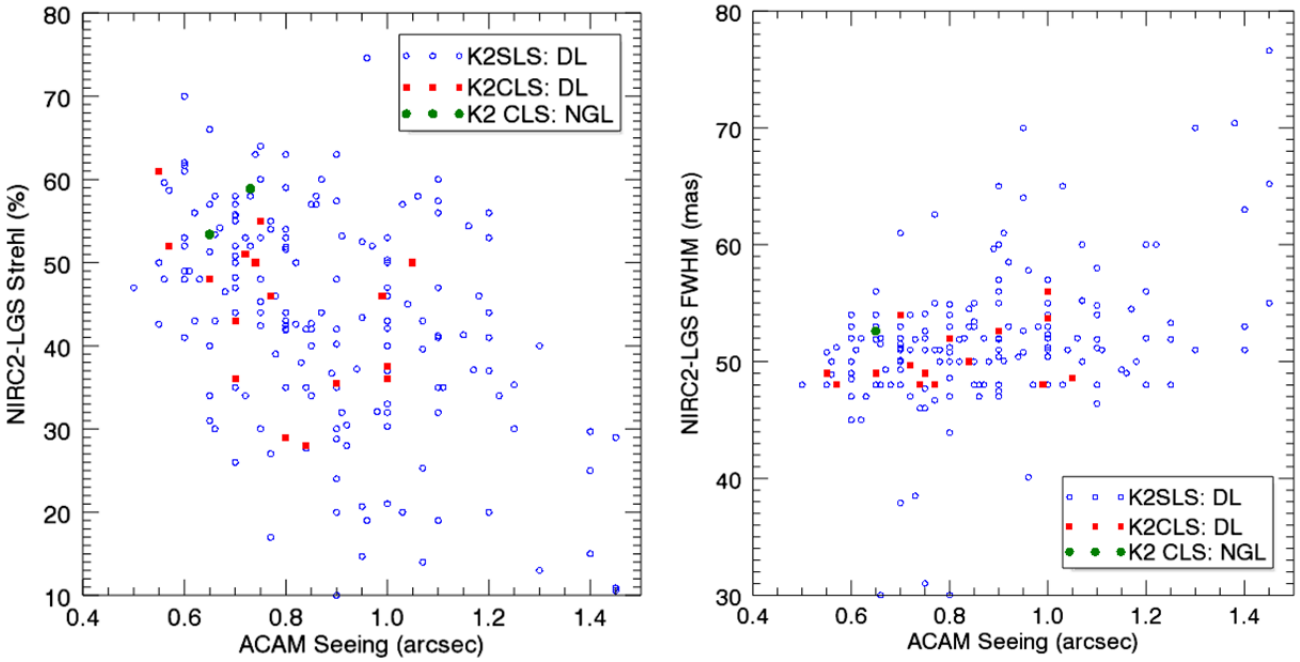

Figure 13: NIRC2 LGS Br γ (λ_{eff} = 2.1685 μm) Strehl ratio (left) and FWHM (right) using CLS and SLS.

The AO performance of the dye laser and the NGL in Br γ filter (λ_{eff} = 2.1685 μm), in terms of Strehl and FWHM in CLS configuration, is compared using dedicated performance measurements (Figure 14 for Strehl ratio and Figure 15 for FWHM). The performance of the NGL under excellent seeing conditions reaches ~ 65% Strehl ratio in Br γ. However, there is significant scatter in the Strehl ratio that is being investigated. Some improvements to the low bandwidth truth wavefront sensor feedback scheme may be needed to fully realize the benefits of reduced asymmetry from CLS. The high frame-rate measurements (1.763 kHz and 2 kHz) give relatively low Strehl ratio compared to 750 Hz and 1000 Hz measurements. This was noticed before in the natural guide star (NGS) case for frame-rates higher than 1.054 kHz. The probable cause for the poor performance at high frame-rate is the system latency and non-optimized WFS clocks.

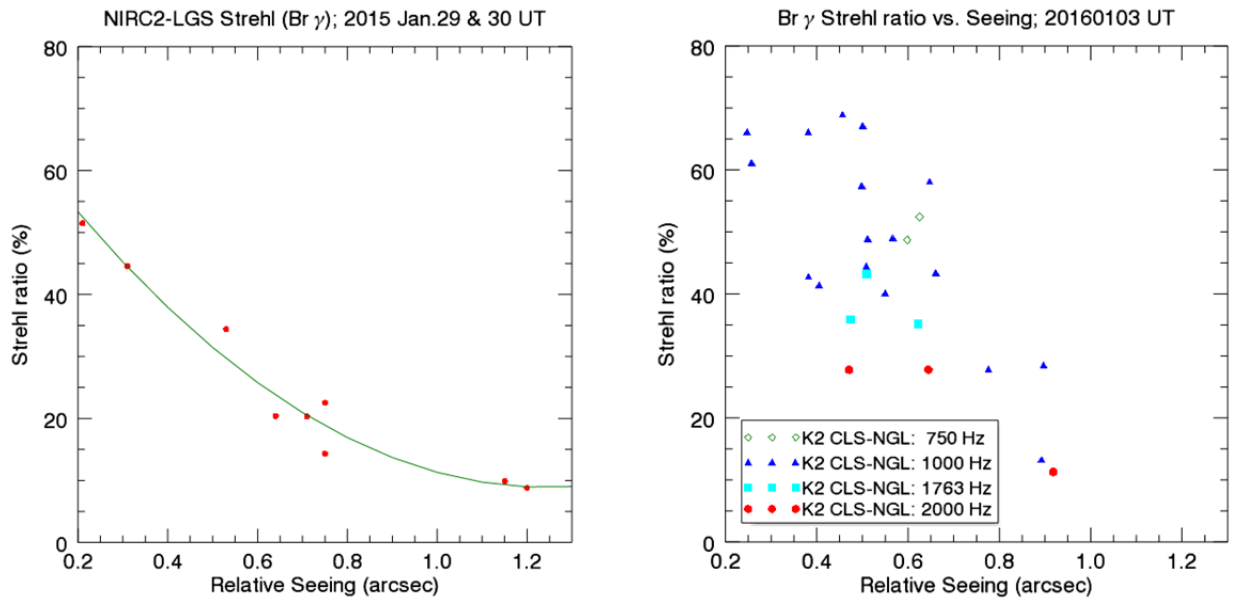

Figure 14: NIRC2 LGS Br γ Strehl with the dye laser (left) and the NGL (right) against relative seeing. The dye laser measurements were taken at 750 Hz.

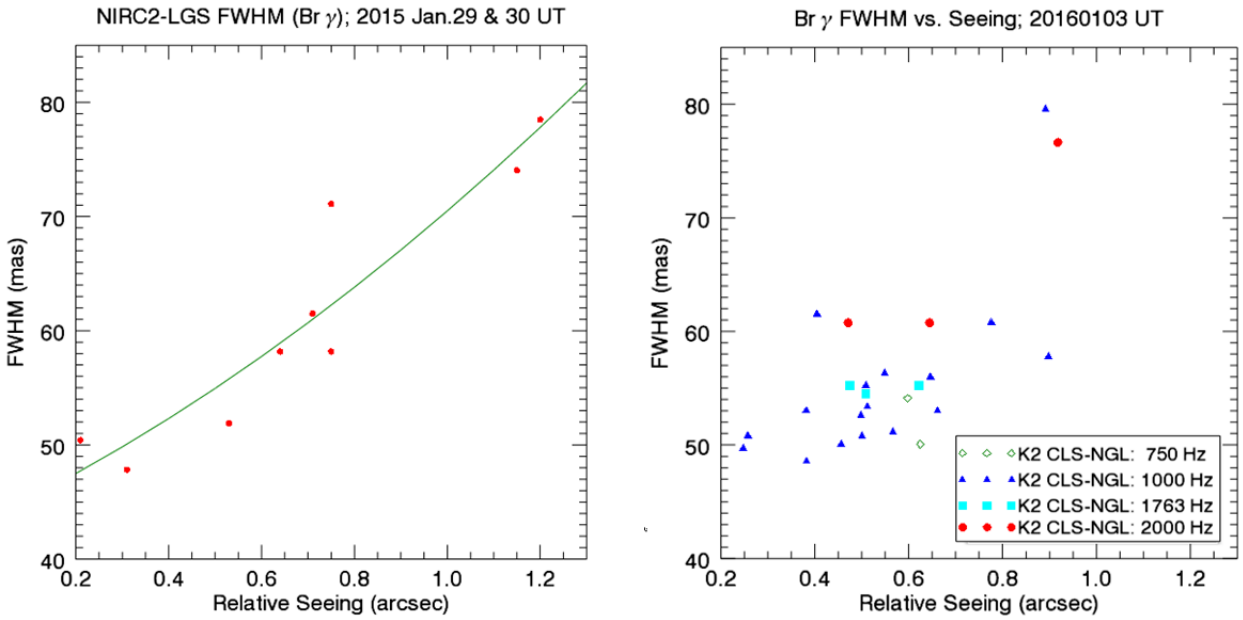

Figure 15: NIRC2 LGS Br γ FWHM with the dye laser (left) and the NGL (right) against relative seeing.

7. SUMMARY AND FUTURE PLANS

The Keck II LGS system is undergoing a major infrastructure upgrade with a new laser delivery system and a new laser. The CLS implementation was completed in 2015 and the commissioning of the TOPTICA/MPBC laser will be complete in early 2016. The new laser with the CLS had first light on Dec. 1, 2015 and the laser was optimized during subsequent engineering runs (2015 Dec. 21 & 27, 2016 Jan. 2 & 4) and some initial performance measurements were made.

The upgraded system routinely provides (1) more compact (FWHM of ~ 1.4" under excellent seeing conditions) and symmetric laser guide star, and (2) an order of magnitude increased laser return (~ a factor of 12 higher than that of the dye laser in SLS configuration and ~ a factor of 19 higher than that of the dye laser in CLS configuration.) Relatively high Strehl ratios of ~ 65% have been achieved under excellent seeing conditions but a large scatter in Strehl ratio is yet to be understood. The system will be further optimized and the performance will be further characterized in order to transition to science operation in April 2016.

The upgraded infrastructure opens up new possibilities for future improvements to the Keck LGS AO system to carryout AO science that was not possible in the past. For instance, the increased laser return could be utilized to reduce the bandwidth noise. This would involve speeding up the WFS hardware (WFS camera, readout electronics, and the data transfer), upgrading the DM and the real-time control system. The high laser return could also be used to separate the laser beam into a three or more LGS asterism to reduce the focal anisoplanatism. Similarly, the improvement to the laser spot symmetry reduces the importance of truth wavefront sensor measurements and could push the limiting magnitude of the NGS guide star required for low bandwidth truth wavefront sensing as relatively low spatial and temporal bandwidth may be adequate. Indeed one may be able to introduce a new operational mode for the faint NGS cases without the truth low bandwidth sensor provided the focus error is derived from the tip-tilt sensor.

ACKNOWLEDGMENTS

The data presented herein were obtained at the W. M. Keck Observatory, which is operated as a scientific partnership among the California Institute of Technology, the University of California, and the National Aeronautics and Space Administration. The Observatory was made possible by the generous financial support of the W. M. Keck Foundation.

This material is based upon work supported by the National Science Foundation (NSF), Gordon and Betty Moore Foundation, the W.M. Keck Foundation, and donors to the W. M. Keck Observatory.

The authors wish to acknowledge the scientific collaborators, Andrea Ghez, Richard Ellis, Michael Lie and Claire Max and several daytime and nighttime staff of the observatory including support astronomers and observing assistants. Special thanks to Liz Chock, Greg Doppmann, Don Holdener, Jim Lyke, Joe Mastromarino and Hien Tran from the Keck Staff, and Matthias Schoeck and Angel Otarola from TMT for their contributions to the project.

The authors wish to recognize and acknowledge the very significant cultural role and reverence that the summit of Mauna Kea has always had within the indigenous Hawaiian community. We are most fortunate to have the opportunity to conduct observations from this mountain.

REFERENCES

- Chin, J., Wizinowich, P., Wetherell, E., Cetre, S., Ragland, S., Campbell, R., Lilley, S., Lyke, J., Medeiros, D., Rampy, R., Stalcup, T., Tsubota, K., Tucker, P., Wei, K. Laser guide star facility developments at W. M. Keck Observatory. SPIE Proc. 9148, 08 (2014).
- Enderlein, M., Friedenauer, A., Schwerdt, R. Rehm, P., Wei, D., Karpov, V., Ernstberger, B., Leisching, P., Clements, W., Kaenders, W. Series production of next-generation guide-star lasers at TOPTICA and MPBC. SPIE Proc. 9148, 07 (2014).
- Wizinowich, P., Acton, D.S., Shelton, C., Stomski, P., Gathright, J., Ho, K., Lupton, W., Tsubota, K., Lai, O., Max, C., Brase, J., An, J., Avicola, K., Olivier, S., Gavel, D., Macintosh, B., Ghez, A., Larkin, J. First Light Adaptive Optics Images from the Keck II Telescope: A New Era of High Angular Resolution Imagery. PASP 112, 315-319 (2000).
- Wizinowich, P., Le Mignant, D., Bouchez, A., Campbell, R., Chin, J., Contos, A., van Dam, M., Hartman, S., Johansson, E., Lafon, R., Lewis, H., Stomski, P., Summers, D., Brown, C., Danforth, P., Max, C., Pennington, D. The W. M. Keck Observatory Laser Guide Star Adaptive Optics System: Overview. PASP 118: 297-309 (2006).